Laminar thermally developing flow in rectangular channels and parallel plates: uniform heat flux

Andrew N. Smith · Horacio Nochetto

Abstract Numerical simulations were conducted for thermally developing laminar flow in rectangular channels with aspect ratios ranging from 1 to 100, and for parallel plates. The simulations were for laminar, thermally developing flow with H1 boundary conditions: uniform heat flux along the length of the channel and constant temperature around the perimeter. In the limit as the non-dimensional length, $x^* = x/(D_h RePr)$, goes to zero, the Nusselt number is dependent on x^* to the negative exponent m. As the non-dimensional length goes to infinity the Nusselt number approaches fully developed values that are independent of x^*. General correlations for the local and mean heat transfer coefficients are presented that use an asymptotic blending function to transition between these limiting cases. The discrepancy between the correlation and the numerical results is less than 2.5 % for all aspect ratios. The correlations presented are applicable to all aspect ratios and all non-dimensional lengths, and decrease the discrepancy relative to existing correlations.

List of symbols

A Area (m^2)
C Correlation coefficient
C_p Fluid specific heat (J/kg K)
D_h Hydraulic diameter (m)
H Channel height (m)
L Channel length (m)
N Blending coefficient
Nu Nusselt number
P Pressure (Pa)
Pr Prandtl number
Re Reynolds number
T Temperature (K)
W Channel width (m)
a Channel half height (m)
a_1 Initial element size (m)
a_n Final element size (m)
b Channel half width (m)
d Incremental element size increase (m)
h Convection heat transfer coefficient (W/m^2 K)
k_f Fluid thermal conductivity (W/m K)
m Correlation exponent
n Number of elements
q Heat transfer (W)
q'' Heat flux (W/m^2)
x^* Dimensionless axial position
u Velocity × direction (m/s)

Greek symbols

α Aspect ratio
ρ Fluid density (kg/m^3)
μ Dynamic viscosity ($N\ s/m^2$)

Subscripts

D Diameter
fd Fully developed
m Mean
s Surface
th Thermally developed
x Local

A. N. Smith (✉)
U.S. Naval Academy, 590 Holloway Road, Annapolis,
MD 21146, USA
e-mail: ansmith@usna.edu

A. N. Smith · H. Nochetto
U.S. Army Research Laboratory, 2800 Powder Mill Road,
Adelphi, MD 20783, USA

1 Introduction

The prevalence of rectangular channels continues to grow with the development of microchannel heat sinks [1, 2] and compact heat exchangers [3]. Whether through microfabrication or conventional machining, rectangular channels are significantly easier to fabricate than round channels on the mini or microscale. As 3D stacking of high power chips becomes a reality, interchip cooling will be required. Brunschwiler et al. [4] demonstrated interlayer cooling in a 3D chip stack using microchannels, parallel plates, and pin fin configurations. As the hydraulic diameter of the channel is decreased, the range of mean velocities over which the flow will be laminar significantly increases. Therefore, accurate correlations for laminar flow in rectangular channels are critical for the future development and application of microchannels for electronics cooling. In addition, there are numerous applications with conventional rectangular channels that would benefit from widely applicable, accurate correlations. Due to the lack of correlations many designers substitute correlations for circular channels which are often not appropriate [1].

While few applications truly exhibit a uniform heat flux along the length of the channel, Lee et al. [1] showed that the H1 boundary condition for thermally developing flow was the most appropriate for microchannel heat sinks. The H1 boundary condition assumes that the perimeter of the channel has a uniform temperature and the heat flux per unit length is uniform along the length of the channel. Correlations for local and mean Nusselt numbers for thermally developing flow were proposed by Lee and Garimella [5] for the H1 boundary condition with aspect ratios of 1–10 and non-dimensional lengths in the entry region. Their correlations are based on computational results for theoretical laminar flow with constant thermophysical properties and are compared to experimental results. It will be shown that these correlations have a maximum discrepancy of 5 % for the local values and 5 % for the mean values with non-dimensional lengths $x* > 1 \times 10^{-3}$. With no additional discrepancy, the Lee and Garimella [5] correlations can be used as $x*$ goes to infinity by transitioning to the fully developed value when the correlation goes below values for fully developed flow. Expressions are available for the fully developed Nusselt number in rectangular channels [6]. The correlations presented by Lee and Garimella [5] should not be extended beyond an aspect ratio of 10 due to the high order polynomials used to determine the coefficients. Wibulswas conducted numerical studies with thermally developing flow with both the H1 boundary condition and the constant temperature, T, boundary conditions [7]. Their results were presented in tabular form for a limited number of non-dimensional lengths and for aspect ratios of 1–4 for the H1 boundary conditions.

Table 1 Thermophysical properties used in the numerical simulations

Density	ρ_f	997.6	kg/m^3
Specific heat	C_p	4,181.5	J/kg K
Thermal conductivity	k_f	0.6056	W/m^3 K
Dynamic viscosity	μ_f	8.55e6	N s/ m^2
Inlet temperature	T_i	293.15	K

2 Thermally developing flow in rectangular channels: numerical simulations

COMSOL was used to conduct a numerical study of thermally developing flow in rectangular channels. The flow velocity profile was assumed to be fully developed and laminar; and the temperature dependence of the thermophysical properties was neglected. Since the velocity profile $u(y, z)$ is known. COMSOL was used to solve the energy equation provided below.

$$\rho_f C_p u \cdot \nabla T = \nabla \cdot \left(k_f \nabla T \right) \tag{1}$$

where C_p is the specific heat, ρ_f is the density and k_f is the thermal conductivity of the fluid, u is the fluid velocity and T is the fluid temperature.

The numerical simulations were conducted on a dimensional basis using the properties of water and geometric dimensions similar to those used by Lee and Garimella [5]. The thermophysical properties used in the simulation are provided in Table 1. The hydraulic diameter was held constant at 333.33 μm while the aspect ratio was varied. The mean velocity was also held constant at 5 m/s throughout the study. By holding the mean velocity, fluid properties and hydraulic diameter constant, the Reynolds number was the same for all aspect ratios. However, since the velocity profile is fully developed and the assumption of the constant thermophysical properties has been made, the calculated Nusselt number is only a function of the non-dimensional length. Several other Reynolds numbers and fluid properties were tested to verify independence.

In the 3D case for rectangular channels, the H1 boundary condition was implemented using a thin wall as the fluid boundary [1]. The thermal conductivity was set to 0 in the axial direction (x) and to a very high value in the lateral directions (y, z). A uniform heat flux was applied to the outer surface of the wall which then results in a constant temperature on the perimeter and uniform heat flux along the length of the channel. In the 2D case for parallel plates, a uniform heat flux was applied at the fluid boundary.

Figure 1 shows a cross section of the model for an aspect ratio of 5. The wall thickness remained constant at 20 μm. Since the channels were rectangular, a mapped mesh was used for both the walls and the fluid channel. The
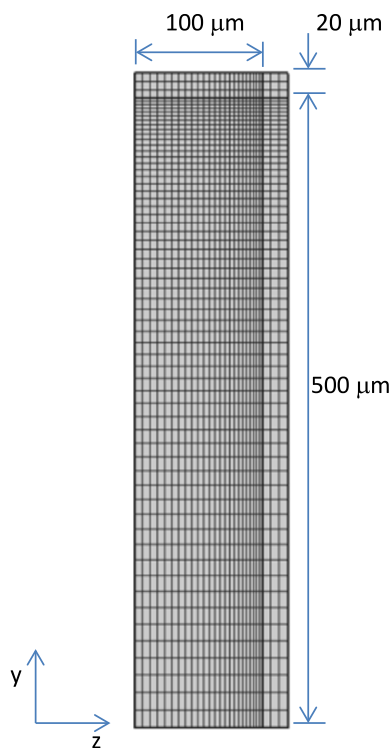
Fig. 1 COMSOL model geometry showing a quarter channel with the thin wall used to implement the H1 boundary condition

final mesh after convergence is also shown in Fig. 1 for the yz cross section. The heat transfer coefficient approaches infinity at the leading edge of the channel, where the thickness of the thermal boundary layer goes to zero. In order to better capture these effects, a non-uniform mesh was used in all directions.

The 3D velocity profile was evaluated based on an analytical expression for fully developed flow shown below as Eq. (2) [8]. The 2D velocity profile was found using the standard equations for Poiseuille flow between parallel plates. The non-uniform mesh used in the study was created using an arithmetic sequence. These relations were used to determine the location of each node within the cross section of the fluid channel. These locations were further refined by creating 4 additional equally spaced points between each node location. The analytical expression for $u(y, z)$ was then evaluated at each point on the refined 2D grid to create 2D table data for the velocity profile.

$$u(y,z) = \frac{-16\left(dP/dx\right)}{\pi^4 \mu_f} \sum_{m=1,3,5...}^{\infty} \sum_{n=1,3,5...}^{\infty} \frac{\sin\frac{m\pi y}{a}\sin\frac{m\pi z}{b}}{mn\left(\frac{m^2}{a^2} + \frac{n^2}{b^2}\right)} \quad (2)$$

where $u(y, z)$ is the fully developed velocity down the channel in the $\times$ direction, $a = H/2$ is the channel half height, $b = W/2$ is the channel half width and μ_f is the dynamic viscosity. The pressure gradient is a constant and

was found in terms of the mean velocity, u_m, by averaging the above expression.

The mean temperature was calculated by integrating the product of the fluid temperature and velocity over the cross section and dividing by the volumetric flow rate. These results were compared to the linear relationship based on a simple energy balance. The two methods agreed to within 1×10^{-4} %. Even though the temperature variation around the perimeter was negligible, the surface temperature at each x position was determined by averaging across the perimeter.

$$T_m = \frac{\int u(y,z)T(y,z)dA}{\int u(y,z)dA} \quad (3)$$

After the original solution was completed, the overall length of each solution was extended by a factor of four by running each converged solution in a pseudo-periodic manner. The outlet temperatures were exported from COMSOL and used as the inlet conditions for a second, third and fourth segment of the channel. The mesh remained identical in the y and z directions, and a uniform element distribution was used in the x direction based on the element width at $x = L$ in the first segment. By using a pseudo-periodic solution, axial conduction in the fluid was neglected at the interface between each segment. The assumption of negligible axial conduction has been commonly applied [5–7], and no discontinuity in the surface temperature or mean temperature was observed. Figure 2 shows the mean and surface temperature profiles for the first and second segments for an aspect ratio of 5. Each segment had a length of 200 mm.

Once the surface and mean temperature profiles were determined, the local and mean heat transfer coefficient
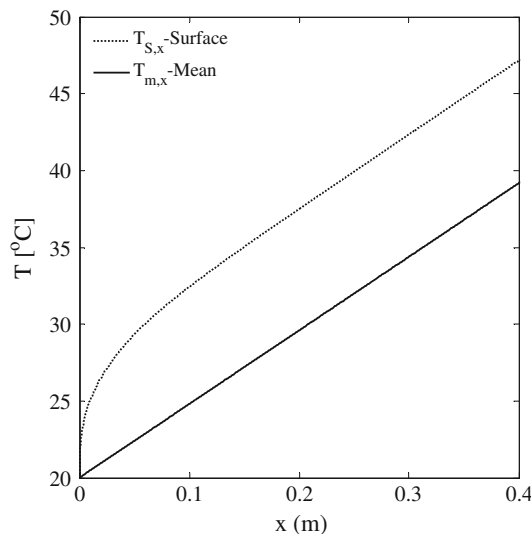

Fig. 2 Surface and mean temperatures for two sequential rectangular channel segments each with an aspect ratio of 5. The dimensions of each channel segment are 1,000 μm × 200 μm × 200 mm

Table 2 Channel dimensions and mesh parameters used for the fluid domain for select aspect ratios

Channel aspect ratio	Channel height (µm)	Channel width (µm)	Channel length (mm)	# y elements	# z elements	# x elements	y growth factor	z growth factor	x growth factor
1	333.33	333.33	400	30	30	2,000	3	3	200
5	1,000	200	200	60	24	1,400	6	3	284
10	1,833.3	183.33	150	90	24	1,200	9	3	124
100	16,833.3	168.33	100	100	24	980	70	3	101
∞		167.77	300		24	2,240		3	268

Table 3 Mesh parameters based on an arithmetic sequence where a_1 is the initial element size and d is the incremental increase

Channel aspect ratio	$a_{1,y}$ (µm)	d_y (µm)	# y elements	$a_{1,z}$ (µm)	d_z (µm)	# z elements	$a_{1,x}$ (µm)	d_x (µm)	# x elements
1	5.55	0.358	30	5.55	0.358	30	2	0.198	2,000
5	4.76	0.390	60	4.17	0.333	24	1	0.202	1,400
10	4.07	0.358	90	3.82	0.306	24	2	0.205	1,200
100	4.74	3.24	100	3.51	0.281	24	2	0.204	980
∞				3.47	0.278	24	1	0.118	2,240

and Nusselt numbers were determined using the following equations.

$$h_x = \frac{\overline{T_{s,x} - T_{m,x}}}{q''}; \quad Nu_{D,x} = \frac{h_x D_h}{k_f} \tag{4}$$

$$\frac{1}{\overline{h_m}} = \frac{1}{L}\int_0^L \frac{1}{h_x}dx; \quad \overline{Nu_{D_h,m}} = \frac{\overline{h_m}D_h}{k_f} \tag{5}$$

where $T_{s,x}$ is the local surface temperature, $T_{m,x}$ is the local mean temperature, q'' is the surface heat flux applied to the channel walls, k_f is the thermal conductivity of the fluid, and L is the channel length.

The non-uniform grid was created with an arithmetic sequence in each direction where the inputs are the number of elements and the factor over which the elements grow over the full range. Table 2 shows the channel dimensions and the mesh input parameters at select aspect ratios for the converged solutions. Table 3 shows the same information as Table 2, but with respect to the arithmetic sequence used to create the non-uniform grid, $a_n = a_1 + (n - 1) \cdot d$, where a_1 is the minimum element size, n is the number of elements and d is the incremental increase. The smallest element is always located in the corner at the inlet and the element dimensions increase in each direction. The very large growth factor in the x direction is necessary to achieve a narrow element at the inlet. The large growth factor has a smaller effect on the size of the final node. In an arithmetic sequence the last node will only increase to twice the average element size as the growth factor goes to infinity.

Mesh convergence was verified in the first segment in the following manner. In each lateral direction the growth factor was held constant and the number of elements was increased by a factor of $\sqrt[3]{2}$ at each refinement. In the axial direction, the element size at x = 0 was decreased by a factor of two, while the number of elements was simultaneously increased by a factor of $\sqrt[3]{2}$ at each refinement. The growth factor in the x direction was then re-calculated based on the first element spacing, number of elements and channel length. While all Nusselt numbers were considered in the convergence criteria, the values at low x^* were the most sensitive to the mesh refinement. The solutions were considered to be converged when the local and mean Nusselt numbers at $x^* = 1 \times 10^{-4}$ did not change by more than 0.1 % as the mesh was refined. The local and mean Nusselt numbers at $x^* = 1 \times 10^{-5}$ changed by less than 0.3 % on the final refinement. To improve the convergence of the mean Nusselt number, the local Nusselt numbers were curvefit over the range of x^* values from 5×10^{-5} to 2×10^{-4} with the functional form Cx^{*m}. The curvefit was then used to approximate the contribution from x^* values below 5×10^{-5} to the mean Nusselt number.

After extending the solution length by a factor of 4, the local Nusselt numbers had reached a constant value. The local fully developed Nusselt values were then compared to the following expression for fully developed flow in rectangular channels developed by Shah and London [6]. The resulting discrepancy was less than ±0.1 %.

$$Nu_{D_h,fd} = 8.235 \cdot \left[1 - 2.0421\left(\tfrac{1}{\alpha}\right) + 3.0853\left(\tfrac{1}{\alpha}\right)^2 \right.$$
$$\left. - 2.4765\left(\tfrac{1}{\alpha}\right)^3 + 1.0578\left(\tfrac{1}{\alpha}\right)^4 - 0.1861\left(\tfrac{1}{\alpha}\right)^5 \right] \tag{6}$$

Having reached thermally fully developed flow, the local heat transfer coefficient was assumed to be constant and extended up to $x^* = 100$. The extended mean heat transfer

coefficients were then calculated up to $x^* = 100$ by integrating over the local heat transfer coefficients using Eq. (5). The results are shown in Figs. 3 and 4. It is clearly observed that the Nusselt numbers of high aspect ratio channels approach the values for parallel plates.

3 Thermally developing flow in rectangular channels: correlations

3.1 Correlations for parallel plates

Shah et al. [9] presented tabulated results for the local and mean Nusselt between parallel plates with a uniform and equal wall heat flux boundary condition based on analytical solutions presented by Cess and Schaffer [10]. Shah proposed the following correlations for the local and mean Nusselt number for thermally developed flow between parallel plates [6].

$$Nu_{D_h,x} = \begin{cases} 1.490 \cdot x^{*-1/3} & x^* \leq 0.002 \\ 1.490 \cdot x^{*-1/3} + 0.4 & 0.002 < x^* \leq 0.01 \\ 8.235 + 8.68(10^3 x^*)^{-0.506} \exp(-164 \cdot x^*) & x^* \geq 0.01 \end{cases} \tag{7}$$

$$\overline{Nu}_{D_h,m} = \begin{cases} 2.236 \cdot x^{*-1/3} & x^* \leq 0.001 \\ 2.236 \cdot x^{*-1/3} + 0.9 & 0.001 < x^* \leq 0.01 \\ 8.235 + \dfrac{0.0364}{x^*} & x^* \geq 0.01 \end{cases} \tag{8}$$

Awad presented correlations based on the tabulated data presented by Shah, but used an asymptotic method to fit the data [11]. Their correlations are provided as Eqs. (9) and (10) for the local and mean Nusselt numbers. The Awad correlation captures the Nusselt number with a single
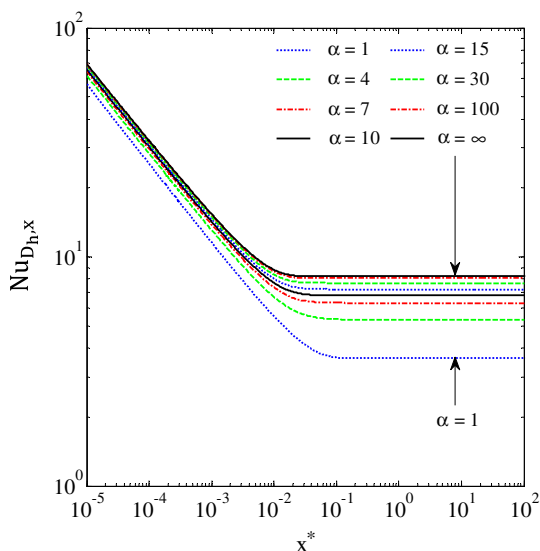

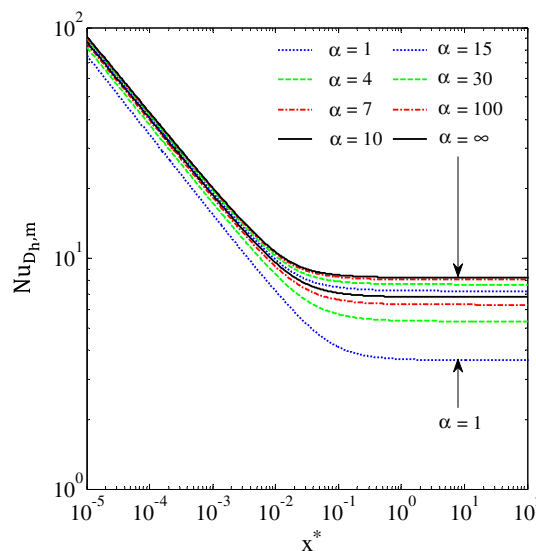Fig. 3 Local Nusselt numbers for thermally developing flow in a rectangular channel with aspect ratio, α

Fig. 4 Mean Nusselt numbers for thermally developing flow in a rectangular channel with aspect ratio, α

equation that transitions from the asymptotic behavior at low values of x^* when the plates are not influencing each other to fully developed flow where the Nusselt number is constant. The asymptotic method was first presented by Churchill and Usagi et al. [12].

$$Nu_{D_h,x} = \left[(1.490 \cdot x^{*-1/3})^{4.5} + (8.235)^{4.5} \right]^{(1/4.5)} \tag{9}$$

$$\overline{Nu}_{D_h,m} = \left[(2.236 \cdot x^{*-1/3})^{3.5} + (8.235)^{3.5} \right]^{(1/3.5)} \tag{10}$$

As discussed in the previous section, COMSOL Multiphysics® was used to solve for the thermally developing temperature profile between parallel plates with a uniform heat flux boundary condition.

Figure 5 compares the analytical Shah tabulated values [9], the Shah correlation [6], the Awad correlation [11], and the current 2D numerical values. The maximum discrepancy between the Shah analytical values and the current 2D numerical simulation is less than ± 0.3 % for x^* values above 5×10^{-5} and less than ± 0.1 % for x^* values above 1×10^{-3} for both the local and mean Nusselt numbers. The Shah correlation has a maximum discrepancy of ± 0.8 % for the local Nusselt number, Eq. (7), and ± 2.6 % for the average Nusselt number, Eq. (8). The Awad correlation has a maximum discrepancy of ± 2.5 % for the local Nusselt number, Eq. (9), and ± 0.9 % for the average Nusselt number, Eq. (10).

The mean Nusselt values presented by Shah are based on a simple average of the heat transfer coefficient. The average heat transfer coefficient derived in this manner is most appropriate when the surface-fluid temperature difference $(T_s - T_m)$ is constant.
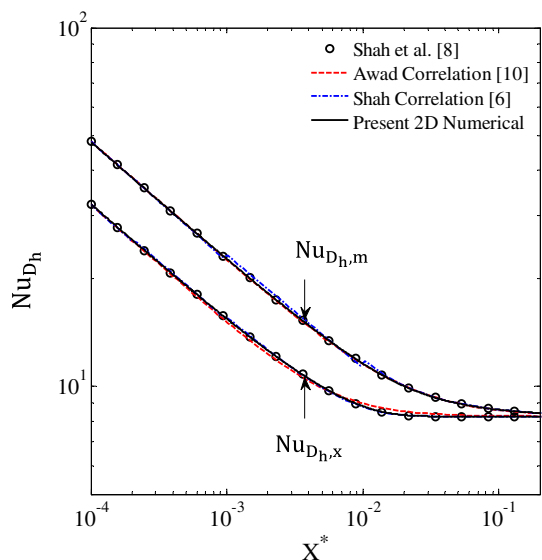
Fig. 5 Comparison of existing correlations and data to a 2D numerical simulation for thermally developing flow between parallel plates with uniform and equal heat fluxes

$$q = \int h_x(T_s - T_m)\,dA = A(T_s - T_m)\frac{1}{A}\int h_x dA$$
$$= \overline{h_m}A(T_s - T_m) \tag{11}$$

where h_x is the local heat transfer coefficient and A is the surface area. The average heat transfer coefficient is then calculated in the following manner.

$$\overline{h_m} = \frac{1}{L}\int_0^L h_x dx \tag{12}$$

An alternative method for calculating the average heat transfer coefficient is based on determining an average temperature difference with a known amount of heat transfer. This method is most applicable when the heat flux, q'', is known and constant [13].

$$\overline{(T_s - T_m)} = \frac{1}{A}\int(T_s - T_m)dA = \frac{1}{A}\int\frac{q''}{h_x}dA$$
$$= q''\frac{1}{A}\int\frac{1}{h_x}dA = \frac{q''}{\overline{h_m}} \tag{13}$$

The mean heat transfer coefficient calculated in this manner represents the average convective resistance of the surface.

$$\frac{1}{\overline{\overline{h_m}}} = \frac{1}{L}\int_0^L \frac{1}{h_x}dx \tag{14}$$

Calculating the mean heat transfer coefficient as an average convective resistance is more appropriate for a constant heat flux boundary condition. Therefore, a new correlation is proposed for the mean Nusselt number to replace Eq. (10). Mean Nusselt numbers were recalculated using Eq.

(14), and a new correlation was developed using the methodology described by Awad et al. [11].

$$\overline{Nu}_{D_h,m} = \left[(1.987 \cdot x^{*-1/3})^{3.5} + (8.235)^{3.5}\right]^{(1/3.5)} \tag{15}$$

3.2 Correlations for rectangular channels: existing

Lee et al. [5] conducted a numerical study for thermal developing flow in channels with aspect ratios from 1 to 10 and channel lengths up to the point where the local Nusselt number was within 5 % of the fully developed values. The results at each aspect ratio were curve fit using an equation with 4 unknown coefficients. The coefficients were then curve fit with polynomials. The resulting correlations are only applicable for aspect ratios up to 10 and for x^* values less than x^*_{th}, the dimensionless entrance length from Eq. (16) [5]. The authors state that for x^* values beyond x^*_{th}, fully developed values according to Eq. (6) should be used. However, it seems more appropriate to transition to the fully developed values when the predicted values fall below the fully developed values.

$$x^*_{th} = -1.275 \times 10^{-6}\alpha^6 + 4.709 \times 10^{-5}\alpha^5 - 6.902 \times 10^{-4}\alpha^4$$
$$+ 5.014 \times 10^{-3}\alpha^3 - 1.769 \times 10^{-2}\alpha^2 + 1.845 \times 10^{-2}\alpha$$
$$+ 5.691 \times 10^{-2} \tag{16}$$

$$Nu_{D_h,x} = \frac{1}{C_{1,x}(x^*)^{C_{2,x}} + C_{3,x}} + C_{4,x} \quad \text{for} \quad 1 \leq \alpha \leq 10$$
$$\text{and} \quad x^* < x^*_{th} \tag{17}$$

$$C_{1,x} = -3.122 \times 10^{-3}\alpha^3 + 2.435 \times 10^{-2}\alpha^2$$
$$+ 2.143 \times 10^{-1}\alpha + 7.325$$
$$C_{2,x} = 6.412 \times 10^{-1}$$
$$C_{3,x} = 1.589 \times 10^{-4}\alpha^2 - 2.603 \times 10^{-3}\alpha + 2.444 \times 10^{-2}$$
$$C_{4,x} = 7.148 - 1.328 \times 10^1\left(\frac{1}{\alpha}\right) + 1.515 \times 10^1\left(\frac{1}{\alpha}\right)^2$$
$$- 5.936\left(\frac{1}{\alpha}\right)^3$$

$$\overline{Nu}_{D_h,m} = \frac{1}{C_{1,m}(x^*)^{C_{2,m}} + C_{3,m}} + C_{4,m} \quad \text{for} \quad 1 \leq \alpha \leq 10 \quad \text{and}$$
$$x^* < x^*_{th} \tag{18}$$

$$C_{1,m} = -2.757 \times 10^{-3}\alpha^3 + 3.274 \times 10^{-2}\alpha^2$$
$$- 7.464 \times 10^{-5}\alpha + 4.476$$
$$C_{2,m} = 6.391 \times 10^{-1}$$
$$C_{3,m} = 1.604 \times 10^{-4}\alpha^2 - 2.622 \times 10^{-3}\alpha + 2.568 \times 10^{-2}$$
$$C_{4,m} = 7.301 - 1.311 \times 10^1\left(\frac{1}{\alpha}\right) + 1.519 \times 10^1\left(\frac{1}{\alpha}\right)^2$$
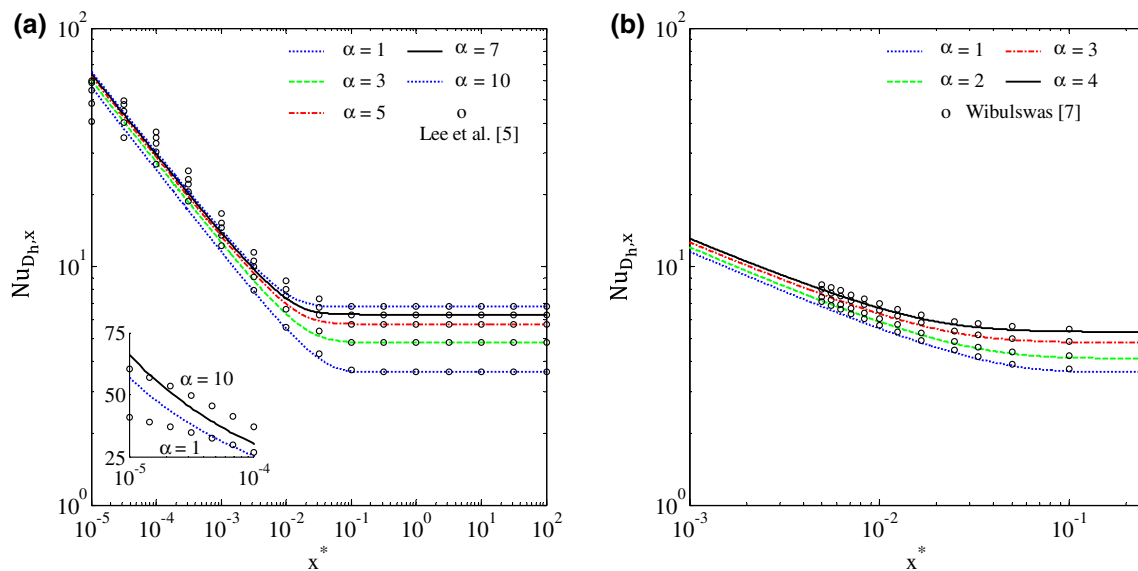$$- 6.094\left(\frac{1}{\alpha}\right)^3$$

Fig. 6 Comparison of local Nusselt numbers with **a** existing correlations for aspect ratios of 1–10 and **b** published values for aspect ratios of 1–4

Figure 6a shows a comparison of the numerical simulations with the local correlations proposed by Lee and Garimella [5]. The Lee correlation is in good agreement with the numerical simulations for $x^* > 1 \times 10^{-3}$ with a maximum discrepancy of less than ± 5 %. The behavior for x^* values below 10^{-4} is more clear visible in Fig. 6a on the inset semi-log plot. At first the Lee correlation begins to overpredict the values, and below $x^* = 1 \times 10^{-4}$ the Lee correlation begins to underpredict as the correlation levels off to a constant value. This is the nature of the functional form chosen for the curvefit, which approaches a constant as x^* goes to zero due to the finite value of C_3 in Eqs. (17) and (18). Therefore, it is recommended that a lower bound be set on the Lee correlations of $x^* = 1 \times 10^{-3}$ for the local correlation. Lee et al. [1, 5] observed that the majority of experimental studies on microchannels experience thermally developing flow where $0.003 \leq x^* \leq 0.056$. Figure 6b shows a comparison between the numerical results and published numerical results of Wibulswas [7]. The agreement was very good, and the small differences are likely attributable to the finer mesh used in this study.

Figure 7a shows a comparison of the numerical simulations with the mean correlations proposed by Lee and Garimella [5]. The agreement between the Lee correlations and the experimental data is very good for $x^* > 1 \times 10^{-4}$ with a maximum discrepancy that is below ± 5 %. The behavior for x^* values below 10^{-4} is shown in Fig. 7a on the inset semi-log plot. The Lee correlation starts to level off and approach a constant value for x^* values below 1×10^{-4}. It is recommended that a lower bound be set on the Lee correlations of $x^* = 1 \times 10^{-4}$ for the mean correlation. Lee and Garimella [5] compared their mean

correlation with experimental data, for x^* values ranging from 3×10^{-4} to 2×10^{-3} with aspect ratios around 5, and showed good agreement. Figure 7b shows a comparison between the current numerical results and the results published by Wibulswas et al. [7]. The lack of agreement in this case stems primarily from the manner in which the mean Nusselt number is calculated. Wibulswas used Eq. (12) to calculate the mean heat transfer coefficient, while the mean value in this study was calculated using Eq. (14) which is consistent with Lee and Garimella [5].

3.3 Correlations for rectangular channels: proposed

The asymptotic method proposed by Churchill and Usagi [12] was used to determine new correlations for the local and mean Nusselt numbers that are applicable for rectangular channels with any aspect ratio subject to the uniform heat flux (H1) boundary condition. The first step was to determine the asymptotic behavior of each aspect ratio as x^* goes to zero. Figure 8 shows the results of the curvefits for the local and mean values with an aspect ratio of 1. As x^* approached infinity, the local and mean Nusselt number approach a constant value which is the fully developed value of 3.61 for an aspect ratio of 1. As x^* approached zero the relationship is clearly linear on a logarithmic plot obeying the following functional form where C and m can be determined from a curvefit.

$$Nu_{D_h, x/m} = Cx^{*m} \qquad (19)$$

The curvefits were used to find C and m at each aspect ratio simulated for both the local and mean Nusselt numbers. The results are provided in Tables 4 and 5. Once the
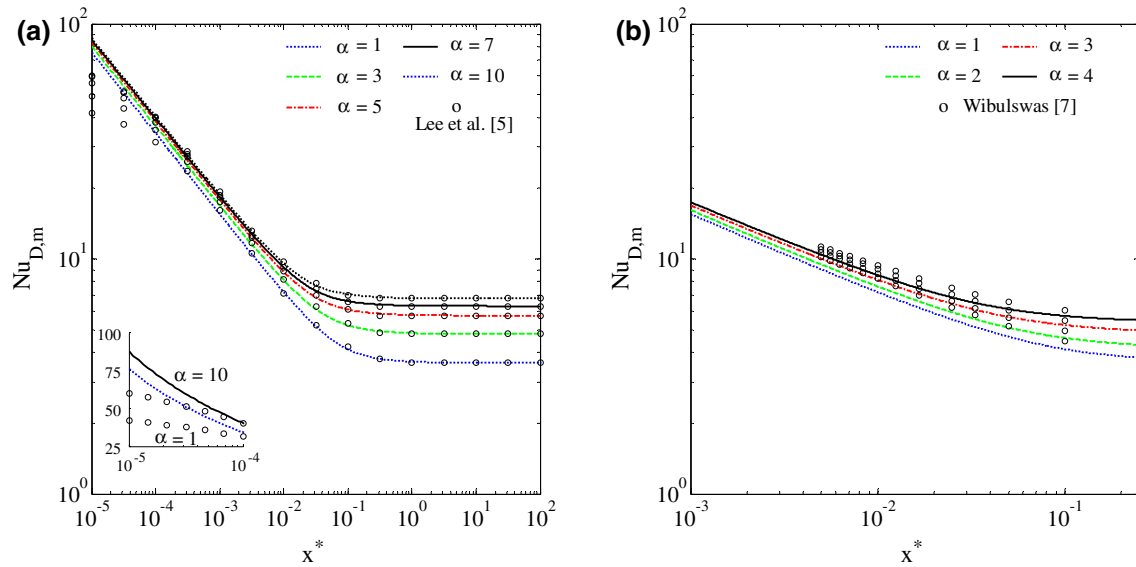
Fig. 7 Comparison of mean Nusselt numbers between **a** existing correlations for aspect ratios of 1–10 and **b** published values for aspect ratios of 1–4
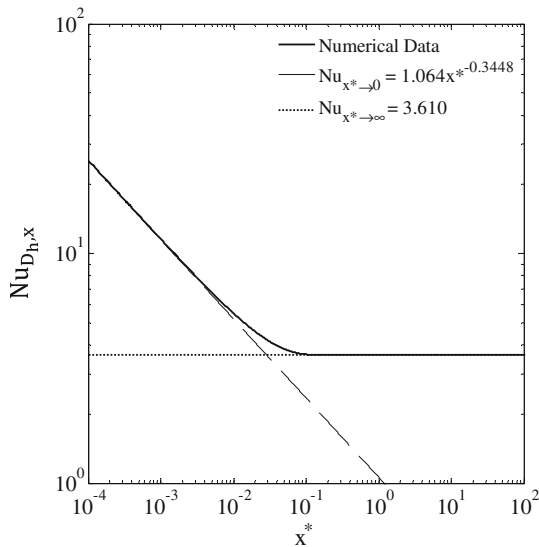

Fig. 8 Curvefit results for the local Nusselt number with an aspect ratio of 1 as $x^* \to 0$ and as $x^* \to \infty$

Table 4 Local Nusselt number curve fit parameters from Eqs. (19) and (20)

α	C	m	N	Nu_{fd}
1	1.064	−0.3448	4.621	3.610
2	1.127	−0.3423	4.411	4.126
3	1.195	−0.3402	4.317	4.798
4	1.248	−0.3386	4.327	5.333
5	1.286	−0.3376	4.358	5.738
6	1.312	−0.3371	4.389	6.050
7	1.333	−0.3367	4.415	6.295
8	1.352	−0.3361	4.451	6.492
9	1.367	−0.3357	4.477	6.654
10	1.380	−0.3353	4.503	6.788
12.5	1.404	−0.3347	4.550	7.042
15	1.422	−0.3342	4.585	7.221
20	1.443	−0.3337	4.620	7.455
30	1.466	−0.3330	4.663	7.702
50	1.486	−0.3325	4.698	7.909
100	1.501	−0.3321	4.722	8.069
∞	1.521	−0.3314	4.761	8.235

asymptotic behavior is known for each limit, the blending function proposed by Churchill and Usagi [12] was used to transition between these two limits.

$$Nu_{D_h} \simeq \left[\left(Nu_{D_h,x^* \to 0}\right)^N + \left(Nu_{D_h,x^* \to \infty}\right)^N \right]^{1/N} \quad (20)$$

The only unknown in this relation is the blending coefficient, N. Figure 9 shows the influence of the blending function on the resulting curvefit. For a blending coefficient of 1 the result is simply the sum of the two functions; however as the blending coefficient goes to infinity the blending function preferentially selects the function with

the larger value when both functions are positive. Since the function $Nu_{D_h,x^* \to 0}$ goes to infinity at $x^* = 0$ and to zero as $x^* \to \infty$, there will only be a single transition. The blending coefficient, N, was determined using a least squares fit in the range of $1 \times 10^{-4} \le x^* \le 1 \times 10^2$ to be 4.621 as shown in Fig. 10. The value of the blending coefficient was determined for each aspect ratio for both the local and mean Nusselt numbers. The results of these curvefits are provided in Tables 4 and 5. It can be observed

Table 5 Mean Nusselt number curve fit parameters for Eqs. (19) and (20)

α	C	m	N	Nu_{fd}
1	1.436	−0.3444	3.524	3.610
2	1.518	−0.3419	3.430	4.126
3	1.612	−0.3495	3.399	4.798
4	1.684	−0.3377	3.416	5.333
5	1.736	−0.3365	3.445	5.738
6	1.773	−0.3359	3.467	6.050
7	1.803	−0.3353	3.488	6.295
8	1.829	−0.3347	3.511	6.492
9	1.849	−0.3343	3.528	6.654
10	1.867	−0.3338	3.544	6.788
12.5	1.900	−0.3331	3.574	7.042
15	1.924	−0.3325	3.598	7.221
20	1.954	−0.3319	3.624	7.455
30	1.986	−0.3312	3.651	7.702
50	2.014	−0.3306	3.673	7.909
100	2.035	−0.3301	3.689	8.069
∞	2.060	−0.3395	3.719	8.235

Fig. 9 Influence of the blending coefficient, N, on the curvefit of the local Nusselt number for an aspect ratio of 1

that the coefficients for the case of parallel plates ($\alpha \rightarrow \infty$) are in agreement with Eqs. (9) and (15) but do not match exactly. This is due to the fact that m and N were determined more exactly from the numerical curve fit described above.

In order to determine a general expression for all aspect ratios, the coefficients C, m and N were plotted as a function of $1/\alpha$ and curvefit with a 2nd or 3rd order polynomial. The resulting correlation is presented for the local Nusselt numbers for rectangular channels with the H1 boundary condition.

$$Nu_{D_h,x} = \left[\left(Nu_{D,x^* \rightarrow 0}\right)^N + \left(Nu_{D,fd}\right)^N \right]^{1/N}$$

$$Nu_{D_h,x^* \rightarrow 0} = 1.515 \left[1 - 0.9991 \left(\frac{1}{\alpha}\right) + 1.263 \left(\frac{1}{\alpha}\right)^2 \right.$$

$$\left. - 0.5613 \left(\frac{1}{\alpha}\right)^3 \right] \cdot x^{*m}$$

$$m = -0.3321 \left[1 + 0.09319 \left(\frac{1}{\alpha}\right) - 0.05564 \left(\frac{1}{\alpha}\right)^2 \right]$$

$$N = 4.688 \left[1 - 0.3647 \left(\frac{1}{\alpha}\right) + 0.3572 \left(\frac{1}{\alpha}\right)^2 \right]$$

$$(21)$$

This correlation is valid for laminar flow, $Re_D < Re_{D,critical}$, in rectangular channels and with fully developed velocity profiles subject to the H1 boundary conditions. Critical Reynolds numbers are between 1,500 and 2,800 for smooth microchannels and between 300 and 700 for rough microchannels [14].

Figure 10 shows the proposed correlation versus the numerical results at a few select aspect ratios. The
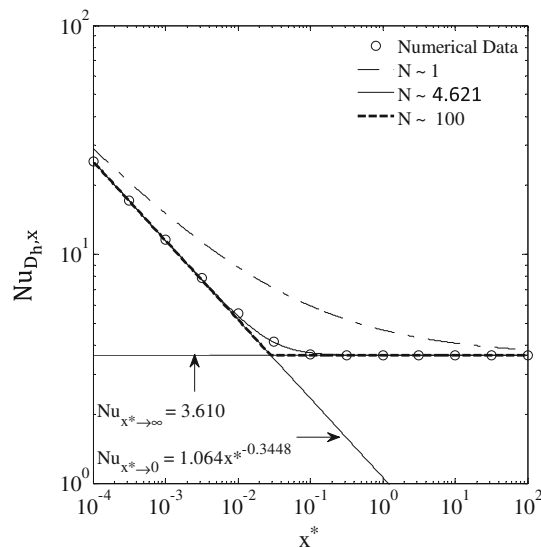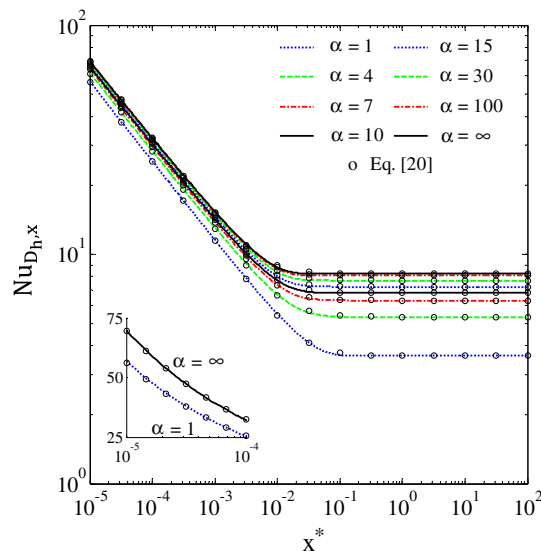

Fig. 10 Comparison of the proposed correlation and the numerical results for local Nusselt numbers

proposed correlation is applicable for all aspect ratios from square channels to parallel plates. The correlation captures the asymptotic relationship as x^* goes to zero and as x^* goes to infinity, therefore the relationship is applicable for all x^* values. There is some discrepancy that arises as the curve transitions between the asymptotic limits, but the maximum discrepancy stays below ±2.5 % which is less than best existing correlations for rectangular channels.

The following correlation is proposed for the mean Nusselt number for rectangular channels subject to the H1 boundary conditions. Figure 11 shows a comparison of the proposed correlation with the numerical results for select
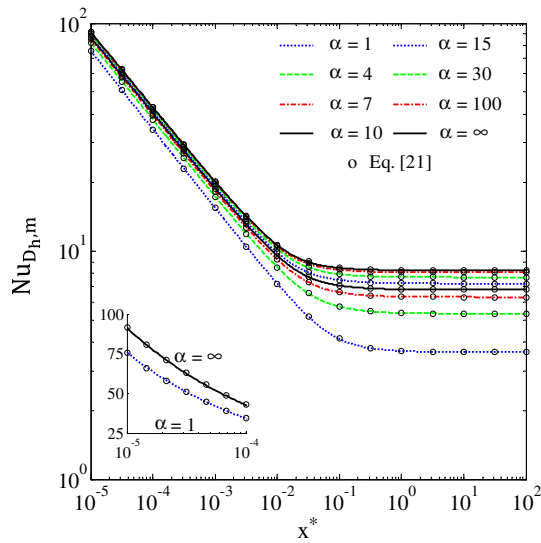
Fig. 11 Comparison of the proposed correlation and the numerical results for mean Nusselt numbers

aspect ratios. Again, since the curve fit captures the asymptotic behavior as x^* goes to zero and as x^* goes to infinity, the correlations is applicable for all x^* values. The maximum discrepancy is less then $\pm 1\%$ for the mean Nusselt numbers.

$$\overline{Nu_{D_h,m}} = \left[\left(\overline{Nu_{D_h,x^*\to 0}}\right)^N + \left(Nu_{D_h,fd}\right)^N\right]^{1/N}$$

$$\overline{Nu_{D_h,x^*\to 0}} = 2.053\left[1 - 1.016\left(\frac{1}{\alpha}\right) + 1.281\left(\frac{1}{\alpha}\right)^2\right.$$
$$\left. - 0.5659\left(\frac{1}{\alpha}\right)^3\right] \cdot x^{*m}$$

$$m = -0.3302\left[1 + 0.1083\left(\frac{1}{\alpha}\right) - 0.06569\left(\frac{1}{\alpha}\right)^2\right]$$

$$N = 3.673\left[1 - 0.3279\left(\frac{1}{\alpha}\right) + 0.2924\left(\frac{1}{\alpha}\right)^2\right]$$

$$(22)$$

4 Conclusions

Numerical simulations were conducted using COMSOL to predict the local and mean Nusselt numbers in the thermally developing region for rectangular channels. The 2D simulations are in excellent agreement with published analytical values for parallel plates by Shah et al. [6]. The 3D numerical simulations are in good agreement with existing correlations by Lee and Garimella [5] for aspect ratios of 1–10 and published numerical values for local Nusselt number [7]. The 3D numerical results approach the parallel plate values as the aspect ratio increases. Existing parallel plate correlations for the mean Nusselt number are based on a simple average, which is most appropriate for constant surface temperature boundary

conditions. While existing rectangular channel correlations for the mean Nusselt number are based on an averaged convective resistance, which is more appropriate when the surface heat flux is constant. A modified correlation is presented for parallel plates based on an average convective resistance.

It has been shown that the existing correlations for rectangular channels, with aspect ratios of 1–10, present by Lee and Garimella [5] agree with the numerical simulations to within $\pm 5\%$ for local when $x^* > 1 \times 10^{-3}$ and mean Nusselt numbers when $x^* > 1 \times 10^{-4}$. New correlations are presented that are applicable for all aspect ratios including parallel plates. The correlations are based on an asymptotic method and therefore more effectively represent the Nusselt number as x^* goes to zero and as x^* goes to infinity. The proposed correlations are applicable for all x^* values and all aspect ratios, and agree with the numerical simulations to $\pm 2.5\%$ for the local correlation and $\pm 1.0\%$ for the mean correlation.

References

1. Lee P-S, Garimella S, Liu D (2005) Investigation of heat transfer in rectangular microchannels. Int J Heat Mass Tran 48:1688–1704
2. Qu W, Mudawar I (2002) Experimental and numerical study of pressure drop and heat transfer in single-phase micro-channel heat sink. Int J Heat Mass Tran 45:2549–2565
3. Kandlikar S (2005) High flux heat removal with microchannels—a roadmap of challenges and opportunities. Heat Transf Eng 26:5–14
4. Brunschwiler T, Michel B, Rothuiezen H, Kloter U, Wunderle B, Oppermann H, Reichl H (2008) Forced convective interlayer cooling in vertically integrated packages. In: Proceedings of 11th intersociety conference on thermal and thermomechancial phenomena in electrical systems, ITHERM 2008, pp 1114–1125
5. Lee P-S, Garimella S (2006) Thermally developing flow and heat transfer in rectangular microchannels of different aspect ratios. Int J Heat Mass Trans 49:3060–3067
6. Shah R, London A (1978) Laminar flow forced convection in ducts. Academic Press, New York
7. Wibulswas P (1966) Laminar-flow heat transfer in non-circular ducts, PhD thesis, University of London
8. Marco S, Han L (1955) A note of limiting laminar Nusselt number in ducts with constant temperature gradient by analogy to thin-plate theory. Trans ASME 77:625–630
9. Shah R (1975) Thermal entry length solutions for circular tubes and parallel plates. In: Proceedings of third national heat mass transfer conference, Indian Institute of Technology, HMT-11-75
10. Cess R, Shaffer E (1959) Heat transfer to laminar flow between parallel plates with a prescribed wall heat flux. Appl Sci Res 8:339–344

11. Awad M (2010) Heat transfer for laminar thermally developing flow in parallel-plates using the asymptotic method. In: Proceedings of thermal issues in emerging technologies, ThETA 3, Cairo, Egypt, pp 371–387

12. Churchill S, Usagi R (1972) A general expression for the correlation of rates of transfer and other phenomena. AlChE J 18:1121–1128

13. Incropera F, Dewitt D, Bergman T and Lavine A (2007) Introduction to heat transfer, 5th edn. Wiley, New York

14. Hetsroni G, Mosyak A, Pogrebnyak E, Yarin L (2005) Fluid flow in micro-channels. Int J Heat Mass Trans 48:1983–1998